

# Neutron-star Radius from a Population of Binary Neutron Star Mergers

Sukanta Bose,<sup>1,2</sup> Kabir Chakravarti,<sup>1</sup> Luciano Rezzolla,<sup>3,4</sup> B. S. Sathyaprakash,<sup>5,6,7</sup> and Kentaro Takami<sup>8,3</sup>

<sup>1</sup>*Inter-University Centre for Astronomy and Astrophysics, Post Bag 4, Ganeshkhind, Pune 411 007, India*

<sup>2</sup>*Department of Physics & Astronomy, Washington State University, 1245 Webster, Pullman, WA 99164-2814, U.S.A*

<sup>3</sup>*Institut für Theoretische Physik, Max-von-Laue-Straße 1, 60438 Frankfurt, Germany*

<sup>4</sup>*Frankfurt Institute for Advanced Studies, Ruth-Moufang-Straße 1, 60438 Frankfurt, Germany*

<sup>5</sup>*Institute for Gravitation and Cosmos, Physics Department, Pennsylvania State University, University Park, PA, 16802, USA*

<sup>6</sup>*Department of Astronomy & Astrophysics, Pennsylvania State University, University Park, PA, 16802, USA*

<sup>7</sup>*School of Physics and Astronomy, Cardiff University, 5, The Parade, Cardiff, UK, CF24 3AA*

<sup>8</sup>*Kobe City College of Technology, 651-2194 Kobe, Japan*

We show how gravitational-wave observations with advanced detectors of tens to several tens of neutron-star binaries can measure the neutron-star radius with an accuracy of several to a few percent, for mass and spatial distributions that are realistic, and with none of the sources located within 100 Mpc. We achieve such an accuracy by combining measurements of the total mass from the inspiral phase with those of the compactness from the postmerger oscillation frequencies. For estimating the measurement errors of these frequencies we utilize analytical fits to postmerger numerical-relativity waveforms in the time domain, obtained here for the first time, for four nuclear-physics equations of state and a couple of values for the mass. We further exploit quasi-universal relations to derive errors in compactness from those frequencies. Measuring the average radius to well within 10% is possible for a sample of 100 binaries distributed uniformly in volume between 100 and 300 Mpc, so long as the equation of state is not too soft or the binaries are not too heavy.

PACS numbers: 04.25.Dm, 04.25.dk, 04.30.Db, 04.40.Dg, 95.30.Lz, 95.30.Sf, 97.60.Jd

*Introduction.* The direct observation of gravitational waves (GWs) by LIGO [1] has increased the expectation that advanced GW detectors will also detect other types of binaries, including binary neutron stars (BNSs). Imprinted in the emitted GWs from such systems is the signature of the equations of state (EOSs) of nuclear matter. For BNSs, this signature manifests itself during the inspiral phase, when the two stars are tidally deformed, and in the postmerger phase, when an unstable hypermassive neutron star (HMNS) can form, emitting GWs at characteristic frequencies [2]. In both cases, however, these imprints will be extremely small and the accuracy of measurement of EOS parameter(s) will be poor, even in detectors like Advanced LIGO (aLIGO) [3] and Advanced Virgo (AdV) [4], unless the binary happens to be nearby.

One way to address this problem is to combine the information in multiple observations [5] with the expectation that the EOS parameter errors will reduce as the number of observations increases. For instance, the tidal deformability parameter would typically go down as the inverse-square-root of the number of BNS detections [6, 7]. Yet, several tens of observations are needed to reduce the errors to a level where only extreme EOSs can be distinguished. An alternative method is to measure the characteristic frequencies of the merger and postmerger signals [8–12]; e.g., the frequency at amplitude maximum,  $f_{\max}$ , correlates closely with the tidal deformability of the two stars [11, 13, 14], and the spectrum of the postmerger GW signal exhibits at least three strong peaks of increasing frequency, dubbed  $f_1$ ,  $f_2$ , and  $f_3$  [10, 11].

In this *Letter*, we explore how well the radius of a neutron star can be measured by utilizing both the inspiral and postmerger phases of the signal from multiple observations. For this purpose, we utilize numerical-relativity simulations to devise an analytical model of the postmerger waveforms

of four reference nuclear-physics EOSs (ALF2, SLy, H4, and GNH3; see [11] for details) in terms of a linear superposition of damped signals with characteristic frequencies  $f_1$  and  $f_2$ . The model allows us to estimate errors  $\Delta f_{1,2}$ , which are very large for individual observations in aLIGO or AdV as the signal-to-noise ratio (SNR) of postmerger oscillations is  $\lesssim 1$  for a source at  $\sim 200$  Mpc. However, the joint error, e.g., in  $f_2$ , for a population of  $\simeq 100$  BNSs, uniformly distributed in the comoving volume between 100 Mpc and 300 Mpc, and observed in the aLIGO-AdV three-detector network, is a few to several percent, depending on the EOS. In essence, for a given binary with average mass  $\bar{M}$  and average radius at infinite separation  $\bar{R}$ , the quasi-universal relations between characteristic frequencies  $f_1$  and  $f_2$  and compactness  $\mathcal{C} := \bar{M}/\bar{R}$  [11, 15] can be used to deduce the error in  $\mathcal{C}$  from the errors in those frequencies, for various masses and mass ratios.<sup>1</sup> Such measurement of  $\mathcal{C}$  can be combined with that of the total-mass from the inspiral to estimate the average radius for a BNS population. We show that for these  $\simeq 100$  BNS observations the error in radius is 2 – 5% for stiff EOSs and 7 – 12% for soft EOSs. Our conclusion is that advanced detectors can help discriminate between stiff and soft EOSs. However, distinguishing two stiff EOSs, will be harder, with additional difficulties for very soft EOSs, whose postmerger signal is considerably weaker.

With important differences, our conclusions broadly agree with those presented recently by other groups. Agathos et al. [7] estimated the evolution of the medians and 95% confidence intervals in the measurement of the leading-

<sup>1</sup> While our analysis utilizes these relations, it is not affected by how strictly universal they are.

order term  $c_0$  in the expansion of the tidal deformability at the reference mass of  $1.35 M_\odot$ , for some reference EOSs in simulated aLIGO data [7] and a Gaussian mass distribution. They found that inspiral signals from  $\approx 100$  or more BNSs are required for determining  $c_0$  to 10% accuracy. Our analysis is different in that instead of constructing Bayesian posteriors of  $c_0$  from the inspiral waveform, we use Monte-Carlo simulations to estimate the mean population radius, but require similar number of sources for discriminating similar pairs of EOSs.

Clark et al. [16] have instead used principal-component analysis to infer the postmerger waveform in various planned or proposed detectors and deduced that in aLIGO the radius of a BNS at a distance of 30 Mpc and with component masses of  $1.35 M_\odot$  each can be estimated to within 430 m, which is a 3 – 4% error. This result appears to agree with our strong-signal case discussed below up to a factor of two. However, their estimates of the postmerger amplitudes are likely affected by the use of more dissipative numerical methods than those employed here and by an approximate treatment of general relativity. We also account for the deterioration in the measurement arising from covariances of BNS masses and the postmerger frequencies values, on the one hand, and the improvement in estimation accuracy that can be had from knowledge of the total-mass from the inspiral phase, on the other hand.

*Postmerger waveforms.* Numerical-relativity simulations have shown that the most likely product of a BNS merger is a metastable HMNS that exists for several tens of milliseconds before collapsing to a rotating black hole [2]. The GWs emitted from such an oscillating, bar-shaped object show a strong correlation with the stiffness of the nuclear material and hence with the EOS [2]. Although also dependent on the total-mass, mass-ratio and EOS, the postmerger GW signal has robust spectral features with prominent peaks at increasing frequencies  $f_1, f_2, f_3$ . These peaks are reminiscent of spectral lines in atomic transitions, so that imprinted in the spectrum of the postmerger signal is the state of dense, nuclear matter. The analogy with atomic spectral lines is broader as it is possible to infer cosmological redshift of a BNS merger from GW observations alone, by measuring the Doppler shift in postmerger spectral peaks of BNS mergers [17].

It is generally accepted that the most prominent peak,  $f_2$  (see Fig. 1), reflects the spin frequency of the  $m = 2$ -deformed HMNS, while the origin of the broader  $f_1$  peak is still under debate. The fact that the  $f_1$  peak is short-lived, disappearing after a few milliseconds, and is accompanied by a symmetric peak at even larger frequencies  $f_3 \sim 2f_2 - f_1$ , supports the interpretation that it is a transient signal produced right after the merger by the damped collisions of the two stellar cores (see [11, 15] for a toy model).

Accurate modeling of waveforms from BNSs requires computationally formidable numerical-relativity calculations. Since we are interested in constraining EOS parameters with extensive Monte-Carlo simulations of signals from  $\simeq 100$  binaries with various EOSs in  $\simeq 100$  noise realizations and aver-

age measurements over hundreds of BNS population realizations, it is clear that the accuracy and costs of the numerical-relativity calculations need to be traded with a less accurate but computationally efficient description of the waveforms. Hence, we derived a phenomenological model for the postmerger waveform using analytical fits in the time domain to a catalogue of numerical-relativity waveforms [11, 15] that can be expressed as a superposition of damped sinusoids with a time-evolving instantaneous frequency [16, 18]:  $h_+(t) = \alpha \exp(-t/\tau_1) [\sin(2\pi f_1 t) + \sin(2\pi(f_1 - f_{1\epsilon})t) + \sin(2\pi(f_1 + f_{1\epsilon})t)] + \exp(-t/\tau_2) \sin(2\pi f_2 t + 2\pi\gamma_2 t^2 + 2\pi\xi_2 t^3 + \pi\beta_2)$ . Here,  $t = 0$  refers to the merger time,  $f_{1\epsilon} = 50$  Hz, and the ansatz reproduces all of the postmerger “+” polarization signals, up to an overall amplitude; this is to be contrasted with the ansatz considered in [18], which models the waveforms only after the amplitudes have decayed to half of the initial values<sup>2</sup>. The above fit not only agrees very well with the signal spectra near  $f_1$  and  $f_2$ , but also with the signal phase in the time-domain, giving matches of  $\sim 80 - 94\%$ . Therefore, when combined with a semi-analytical model of the inspiral waveform, e.g., via a post-Newtonian expansion with tidal corrections, the fitting ansatz gives a complete analytic description of the signal from merging BNSs. The above fit, parameterized by eight parameters (see Table I in the supplemental material), produces an accurate representation of the waveform phase and a reasonably good description of its amplitude. The top panels in Fig. 1 show numerical-relativity amplitude  $h_+(t)$  and the analytical fits for four different EOSs and for sources at 50 Mpc. The bottom panels show the corresponding spectral amplitudes,  $2\sqrt{f}|\tilde{h}(f)|$ , and the sensitivity curves of aLIGO and the Einstein Telescope [20]. Here  $\tilde{h}(f)$  is the Fourier transform of  $h_+(t)$ ,

Two remarks are in order: First, the four EOSs chosen provide a good coverage of the plausible range in stiffness of nuclear matter, but do not represent very soft EOSs, such as APR4 [21]. The corresponding postmerger signal is much more complex [11, 15], with beats between different frequencies not reproduced with our simple fitting ansatz. Second, our fits best represent equal-mass systems and although the masses in observed binaries do not differ significantly, it is unlikely that LIGO sources have mass ratio  $q = 1$ . Nevertheless, the quasi-universal relations used here continue to be valid also for systems with mass ratio  $q \gtrsim 0.8$  [11, 15].

Our analytic waveforms also facilitate the interpretation of the Monte-Carlo results described below in terms of the Fisher information matrix parameter estimates, which broadly agree with the former (see Table I in the supplemental material), except for the soft EOSs. For a source even at 50 Mpc, the postmerger signal alone will be difficult to *detect* in an aLIGO detector. As an example, the postmerger waveform of the H4 binary with average mass  $1.325 M_\odot$  (H4-1325) has

<sup>2</sup> Better matches can be obtained by including more terms and parameters in the ansatz; however, the main effect of a less than perfect match is a lower SNR; see also Ref. [19] for an alternative ansatz.

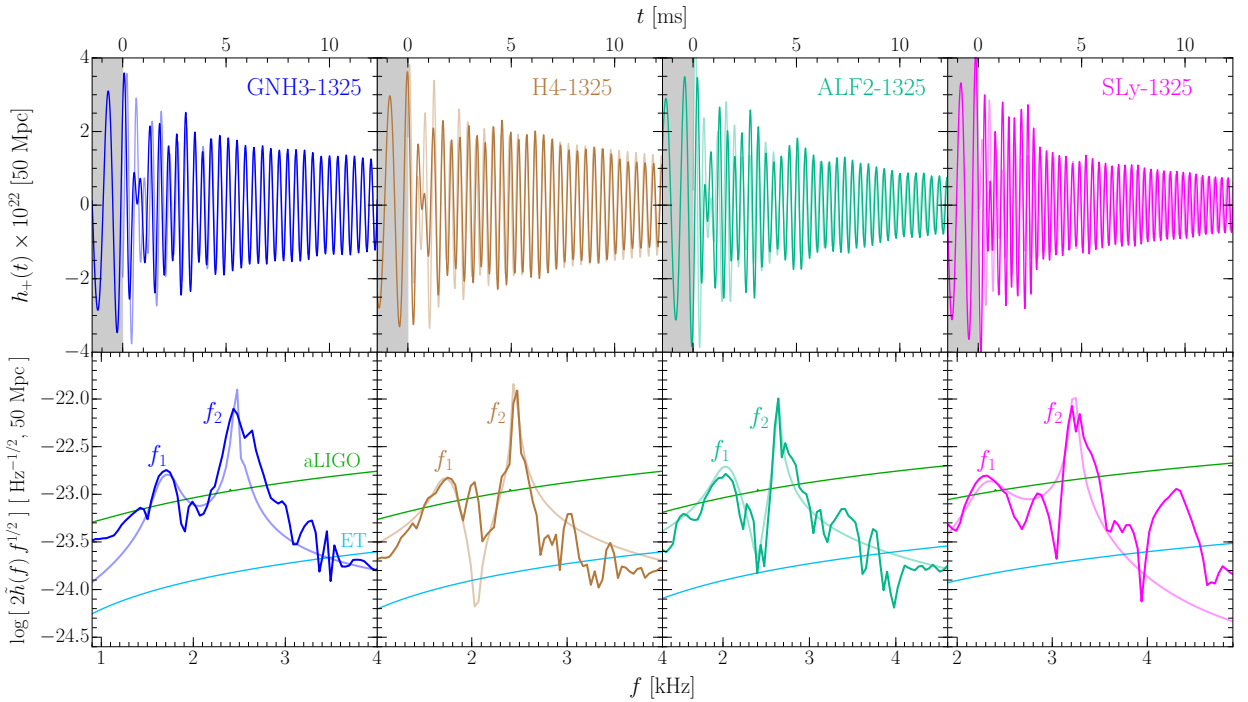


FIG. 1. *Top panels:* Postmerger strain from numerical-relativity waveforms for four EOSs and a representative mass of  $\bar{M} = 1.325 M_{\odot}$ ; our analytical ansatz is shown as a transparent line of the same color. Only the initial 12 ms of the complete 25 ms waveforms are reported to aid the comparison. *Bottom panels:* Corresponding spectral amplitudes shown with the same color convention, superposed on the strain sensitivity curves of aLIGO and ET. Similarly good matches are produced also for  $\bar{M} = 1.250 M_{\odot}$  (cf. Table I and Fig. 3 in the supplemental material).

$|2\tilde{h}(f) f^{1/2}| \simeq 10^{-22}/\sqrt{\text{Hz}}$  at  $f = f_2 \simeq 2470$  Hz, with the frequency bin-width being  $\delta f \sim 100$  Hz. The aLIGO noise amplitude at this frequency is  $S_h(f_2) \simeq 1.26 \times 10^{-46} \text{ Hz}^{-1}$ , thus yielding an SNR  $\simeq |2\tilde{h}(f) f^{1/2}|[\delta f/(f S_h(f))]^{1/2} \simeq 1.8$ .

A small postmerger SNR, however, does not necessarily imply that the observations contain no information. Rather, small-SNR postmergers can provide constraints if combined constructively over a population of such signals. As an example, a Fisher-matrix analysis gives the  $1 - \sigma$  error in measuring  $f_1$  and  $f_2$  for a population of 100 H4-1325 BNSs at 100 Mpc with optimal sky-position and orientation to be  $\Delta f_1/f_1 \simeq 10\%$  and  $\Delta f_2/f_2 \simeq 1\%$ , or  $\Delta f_1 \simeq 177$  Hz and  $\Delta f_2 \simeq 27$  Hz in a single aLIGO detector (see Table I in the supplemental material). Exploiting the quasi-universal relations between  $f_1$ ,  $f_2$  and the compactness (see the left two panels in Fig. 2 in the supplemental material), we can infer the error in  $\mathcal{C}$  through error propagation. For the aforementioned 100 BNS observations, we deduce from the error in  $f_2$  (which is much better measured than  $f_1$ ) that the fractional error in the measurement of the compactness is as small as  $\approx 1.0\%$ . Similar results are obtained for the other EOSs, and masses and are listed in Table I in the supplemental material. We have also verified that other fitting expressions for  $f_1$ ,  $f_2$ , e.g., in terms of fractional powers of  $\mathcal{C}$ , yield very similar errors in the radius estimates derived below.

*Radius measurement from a single BNS.* For the H4-1325 BNS at 200 Mpc, with an aLIGO-AdV network SNR = 14 for the complete inspiral-merger-postmerger signal (after averaging over sky locations and orientations, which reduces the SNR by a factor of 2.26 relative to that for optimal sky location and orientation [5, 22]), the  $1 - \sigma$  measurement errors are  $\Delta f_2/f_2 \approx 14.0\%$  (Table I in the supplemental material), and derived from it via quasi-universal relations,  $\Delta \mathcal{C}/\mathcal{C} \approx 9\%$ . Taking the component mass  $1 - \sigma$  error to be 11% [23], the error in radius from error propagation is  $\approx 14\%$ . For the same source at 30 Mpc with optimal location and orientation, the complete-waveform network-SNR will be  $\approx 211$ , even though the postmerger signal will have SNR  $\approx 6.4$ . At such a distance, the error in average binary mass is much smaller, at 0.08%, and  $\Delta \mathcal{C}/\mathcal{C} \approx 0.9\%$ . In this strong-signal case, the radius error reduces to  $\approx 0.9\%$ , or 125 m. In a single aLIGO detector, the error will rise to  $\approx 215$  m. This is roughly two times more accurate than the value given in Ref. [16], the primary reason being that their waveforms are more rapidly damped than ours, as noted above. Furthermore, while our errors are estimated for the average radius of the parent BNS, the error in Ref. [16] is estimated for the radius of a cold nonrotating neutron star of mass  $1.6 M_{\odot}$  ( $R_{1.6}$ ) and for a single value of the average mass ( $\bar{M} = 1.350 M_{\odot}$ ); we find this approach not applicable to our data and that of other groups (see Fig. 5 in the supplemental material). Finally, other constraints can be

imposed from the quasi-universal relation that exists between the stellar compactness and the tidal deformability parameter  $\kappa_2^T$  (see Fig. 1 in the supplemental material), which introduces additional quasi-universal relations between  $f_1$ ,  $f_2$  and  $\kappa_2^T$ .

*Radius measurement from a BNS population.* At such small SNRs it is not possible to measure  $f_{1,2}$  accurately. However, for a population of  $N > 1$  BNSs it is possible to align and stack the  $f_2$  peaks, so that for a large enough  $N$ , and uncorrelated noise across those  $N$  observations, the stacked amplitude spectra can have enough SNR to allow for an accurate measurement of  $f_2$ . A realistic population will have a variety of mass pairs, but since the total-mass of a BNS system correlates well with  $f_2$  [15, 24], one can use a measurement of  $M_{\text{tot}} = 2\bar{M}$  from the inspiral waveform to deduce it. To test this idea, we performed a Monte-Carlo simulation (see supplementary materials) comprising multiple time-series, each with a simulated postmerger signal from this BNS population added to Gaussian noise with aLIGO zero-detuned-high-power noise power-spectral density [25]. Similar to Ref. [16], we rescaled the multiple signal spectra to align the  $f_2$  values deduced from the (generally erroneous) total-mass estimate for each signal to stack all at a chosen common frequency,  $f_2^c$ . Standard spectral frequency estimation yielded the value of  $f_2^c$  and its statistical spread for that population. We next used the quasi-universal relation between  $f_2$  and compactness, and error-propagation, to deduce the error in the average neutron-star radius of that population.

In our Monte-Carlo simulations, each experiment employed 100 BNS postmerger signals injected in 100 uncorrelated time-series of Gaussian noise with aLIGO zero-detuned-high-power noise power-spectral density. The stacking method described above was used to deduce  $f_2^c$  for this experiment. We repeated this hundred times by changing only the noise realizations and found the mean  $f_2^c$ , and its 90% confidence interval, for this experiment ensemble. Finally, to keep error fluctuations to less than a percent, we computed the average confidence interval over 900 copies of experiment ensembles by changing the BNS sources (within the chosen range of masses and distances) and noise realizations.

Since the mass distribution of extragalactic BNSs is not known, we study two different populations. In the first case we took the masses to be uniformly distributed in a range listed below. In the second case, we built a large set of normally distributed masses centered at  $1.35 M_\odot$ , with standard-deviation  $0.05 M_\odot$ , to mimic the masses in galactic BNSs [7]. We then drew our sample of  $2N$  masses from this distribution by restricting them to lie within a given range.

For all EOSs and the two mass distributions (Gaussian and uniform) the radius errors found from Monte-Carlo studies are similar to those obtained from Fisher studies, provided one limits the masses to the range  $[1.2, 1.38] M_\odot$  (see Fig. 2); the notable exception is the error for the Gaussian distribution with the SLy EOS. The reason for the agreement with the Fisher-matrix estimates is that the average value of  $f_2$  is not very high. However, for the Gaussian mass distribution for SLy, the average  $f_2$  is the highest, so that for the same per-

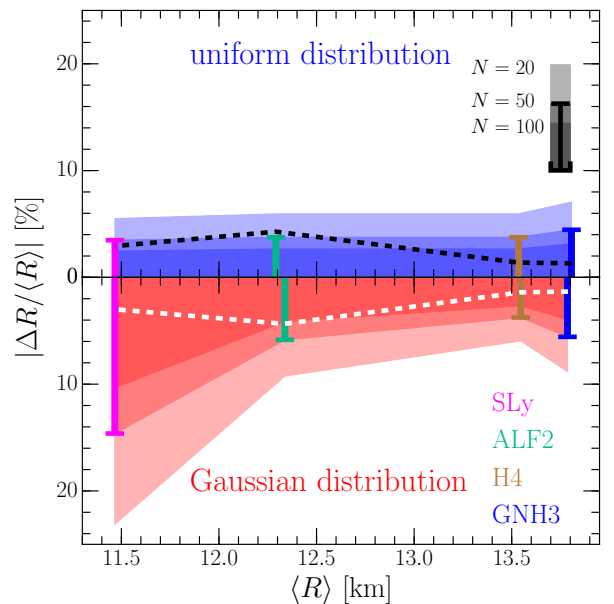


FIG. 2. Estimated relative error in the radius measured, at 90% confidence level, versus the average population radius for different EOSs and  $N = 20, 50, 100$  (different shadings) BNSs distributed uniformly in a comoving volume between 100 and 300 Mpc. The two panels refer to binaries whose distribution in mass in the range  $[1.2, 1.38] M_\odot$  is either uniform (top) or Gaussian (bottom). Shown with dashed lines are the errors from the Fisher-matrix analysis for  $N = 50$ .

centage error in  $f_2$ , the error  $\Delta f_2$  is largest for SLy. This implies that the stacking of signals works less perfectly and the summed signal at the fiducial frequency grows slower with the number of observations than what is realized in the Fisher method. To confirm this behaviour, we considered two sets of Monte-Carlo simulations, one with the same population of 100 BNSs but with all masses set to  $1.25 M_\odot$ ; in the second one we took the masses to be  $1.325 M_\odot$ . For the SLy EOS, we found that the radius error is about 2.7% for the first (low-mass) case, but rises to about 10% for the second (high-mass) case, at 90% confidence level.

From Fig. 2 it is clear that as the EOS gets softer, the Fisher-matrix errors will be less credible and that if the EOS turns out to be soft, then measuring the radius to an accuracy of 10% will be challenging with aLIGO-like detectors.

*Conclusions.* We have presented a new method to infer the average radius of a population of neutron stars in BNSs that employs both the inspiral-merger and the postmerger phases, and that may provide us with a useful alternative to the one where it is inferred from the tidal corrections to the inspiral-merger phase alone. In particular, the postmerger phase allows for the measurement of the compactness, which nicely complements the measurement of the component masses via the inspiral phase to help us determine the radius. Hence, our phenomenological time-domain modeling of the postmerger waveform can prove handy for the production of complete in-

spiral, merger and postmerger time-domain waveforms.

It may be argued that our results are somewhat limited for at least two reasons. First, our phenomenological fits and the estimates of the errors  $\Delta f_{1,2}$  are given for binaries with mass ratio  $q \simeq 1$ . However, we have found that similar fits can be obtained for unequal mass-ratios studied in [15], and that  $\Delta f_{1,2}$  are very similar in such cases for signals with the same SNRs. This observation is consistent with those made in [16]. If nature relents to provide us with an especially strong signal, such that the network SNR of the postmerger signal is  $\approx 6.4$ , which can happen if the source is of optimal orientation and sky-position, and located at a distance of 30 Mpc, then our method can be used to deduce the radius to about 1.6%, at 90% confidence level. Second, as the number of observed binaries increases and the fractional errors of the EOS properties decrease, the systematic uncertainties, mostly related to the accuracy of numerical-relativity calculations, will become the dominant source of errors. While this is somewhat inevitable as the simulations are still too expensive to provide Richardson-extrapolated results, or to include the most sophisticated treatments of magnetic-field growth and neutrino emission, progress is continuously made on this front and the results that will be obtained in the coming decade will significantly reduce the impact of these systematic uncertainties.

Finally, since both the imprint of EOS and the signals themselves may be weak, it will be important to utilize as much of the signal as is meaningful for measuring the EOS parameters. This can be especially helpful owing to the possibility that these parameters may have non-trivial covariances with other parameters, such as their masses. EOS estimation would therefore gain from exploring if the same EOS parameter values can explain consistently features in all parts of the waveform, specifically, the inspiral and the postmerger waveforms.

*Acknowledgements.* It is a pleasure to thank J. Clark, B. Lackey and J. Read for reading the manuscript and providing useful input. Support comes from: NSF grants (PHY-1206108, PHY-1506497); ERC Synergy Grant “Black-HoleCam” (Grant 610058); “NewCompStar”; COST Action MP1304; LOEWE-Program in HIC for FAIR; European Union’s Horizon 2020 Research and Innovation Programme (Grant 671698) (call FETHPC-1-2014, project ExaHyPE); JSPS KAKENHI grant (Grant 15H06813, 17K14305); and the Navajbai Ratan Tata Trust. The simulations were performed on SuperMUC at LRZ-Munich, on LOEWE at CSC-Frankfurt and on Hazelhen at HLRS in Stuttgart. This manuscript was assigned the LIGO Document No. [ligo-p1700071](#).

---

[1] B. P. Abbott, R. Abbott, T. D. Abbott, M. R. Abernathy, F. Acernese, K. Ackley, C. Adams, T. Adams, P. Addesso, R. X. Adhikari, and et al., *Phys. Rev. Lett.* **116**, 061102 (2016), [arXiv:1602.03837 \[gr-qc\]](#)  
 [2] L. Baiotti and L. Rezzolla, [arxiv:1607.03540](#) (2016), [arXiv:1607.03540 \[gr-qc\]](#)

[3] J. Aasi *et al.* (LIGO Scientific), *Class. Quant. Grav.* **32**, 074001 (2015), [arXiv:1411.4547 \[gr-qc\]](#)  
 [4] F. Acernese *et al.* (VIRGO), *Class. Quant. Grav.* **32**, 024001 (2015), [arXiv:1408.3978 \[gr-qc\]](#)  
 [5] J. Abadie, B. P. Abbott, R. Abbott, M. Abernathy, T. Accadia, F. Acernese, C. Adams, R. Adhikari, P. Ajith, B. Allen, and et al., *Class. Quantum Grav.* **27**, 173001 (2010), [arXiv:1003.2480 \[astro-ph.HE\]](#)  
 [6] W. Del Pozzo, T. G. F. Li, M. Agathos, C. Van Den Broeck, and S. Vitale, *Phys. Rev. Lett.* **111**, 071101 (2013), [arXiv:1307.8338 \[gr-qc\]](#)  
 [7] M. Agathos, J. Meidam, W. Del Pozzo, T. G. F. Li, M. Tompitak, J. Veitch, S. Vitale, and C. Van Den Broeck, *Phys. Rev. D* **92**, 023012 (2015), [arXiv:1503.05405 \[gr-qc\]](#)  
 [8] A. Bauswein and H.-T. Janka, *Phys. Rev. Lett.* **108**, 011101 (2012), [arXiv:1106.1616 \[astro-ph.SR\]](#)  
 [9] N. Stergioulas, A. Bauswein, K. Zagkouris, and H.-T. Janka, *Mon. Not. R. Astron. Soc.* **418**, 427 (2011), [arXiv:1105.0368 \[gr-qc\]](#)  
 [10] K. Takami, L. Rezzolla, and L. Baiotti, *Phys. Rev. Lett.* **113**, 091104 (2014), [arXiv:1403.5672 \[gr-qc\]](#)  
 [11] K. Takami, L. Rezzolla, and L. Baiotti, *Phys. Rev. D* **91**, 064001 (2015), [arXiv:1412.3240 \[gr-qc\]](#)  
 [12] S. Bernuzzi, T. Dietrich, and A. Nagar, *Phys. Rev. Lett.* **115**, 091101 (2015), [arXiv:1504.01764 \[gr-qc\]](#)  
 [13] J. S. Read, L. Baiotti, J. D. E. Creighton, J. L. Friedman, B. Giacomazzo, K. Kyutoku, C. Markakis, L. Rezzolla, M. Shibata, and K. Taniguchi, *Phys. Rev. D* **88**, 044042 (2013), [arXiv:1306.4065 \[gr-qc\]](#)  
 [14] S. Bernuzzi, A. Nagar, S. Balmelli, T. Dietrich, and M. Ujevic, *Phys. Rev. Lett.* **112**, 201101 (2014), [arXiv:1402.6244 \[gr-qc\]](#)  
 [15] L. Rezzolla and K. Takami, *Phys. Rev. D* **93**, 124051 (2016), [arXiv:1604.00246 \[gr-qc\]](#)  
 [16] J. A. Clark, A. Bauswein, N. Stergioulas, and D. Shoemaker, *Class. Quantum Grav.* **33**, 085003 (2016), [arXiv:1509.08522 \[astro-ph.HE\]](#)  
 [17] C. Messenger, K. Takami, S. Gossan, L. Rezzolla, and B. S. Sathyaprakash, *Phys. Rev. X* **4**, 041004 (2014)  
 [18] J. Clark, A. Bauswein, L. Cadonati, H.-T. Janka, C. Pankow, and N. Stergioulas, *Phys. Rev. D* **90**, 062004 (2014), [arXiv:1406.5444 \[astro-ph.HE\]](#)  
 [19] K. Hotokezaka, K. Kiuchi, K. Kyutoku, T. Muranushi, Y.-i. Sekiguchi, M. Shibata, and K. Taniguchi, *Phys. Rev. D* **88**, 044026 (2013), [arXiv:1307.5888 \[astro-ph.HE\]](#)  
 [20] M. Punturo *et al.*, *Class. Quantum Grav.* **27**, 194002 (2010)  
 [21] A. Akmal, V. R. Pandharipande, and D. G. Ravenhall, *Phys. Rev. C* **58**, 1804 (1998), [arXiv:hep-ph/9804388](#)  
 [22] S. Ghosh and S. Bose, (2013), [arXiv:1308.6081 \[astro-ph.HE\]](#)  
 [23] C. L. Rodriguez, B. Farr, V. Raymond, W. M. Farr, T. B. Littenberg, D. Fazi, and V. Kalogera, *Astrophys. J.* **784**, 119 (2014), [arXiv:1309.3273 \[astro-ph.HE\]](#)  
 [24] A. Bauswein, H.-T. Janka, K. Hebeler, and A. Schwenk, *Phys. Rev. D* **86**, 063001 (2012), [arXiv:1204.1888 \[astro-ph.SR\]](#)  
 [25] LIGO Technical Report LIGO-T0900288-v3, “Ligo document control center (2010),” <https://dcc.ligo.org/cgi-bin/DocDB/ShowDocument?docid=2974>

## SUPPLEMENTAL MATERIAL

The purpose of this Appendix is to summarize the existence of the quasi-universal relations that have been employed in the Fisher matrix analysis and the Monte-Carlo simulations described in the main text. Although most of the information on these relations has been presented in a number of previous publications [10, 11, 15], it is useful to summarize it here.

We start by recalling some definitions. The tidal deformability parameter  $\kappa_2^T$  for a generic unequal-mass binary is defined as

$$\kappa_2^T := 2 \left[ q \left( \frac{X_A}{C_A} \right)^5 k_2^A + \frac{1}{q} \left( \frac{X_B}{C_B} \right)^5 k_2^B \right], \quad (1)$$

where  $A$  and  $B$  refer to the primary and secondary stars in the binary,

$$q := \frac{M_B}{M_A} \leq 1, \quad X_{A,B} := \frac{M_{A,B}}{M_A + M_B}, \quad (2)$$

$k_2^{A,B}$  are the  $\ell = 2$  dimensionless tidal Love numbers, and  $C_{A,B} := M_{A,B}/R_{A,B}$  are the compactnesses. In the case of equal-mass binaries,  $k_2^A = k_2^B = \bar{k}_2$ , and expression (1) reduces to

$$\kappa_2^T := \frac{1}{8} \bar{k}_2 \left( \frac{\bar{R}}{\bar{M}} \right)^5 = \frac{3}{16} \Lambda = \frac{3}{16} \frac{\lambda}{\bar{M}^5}, \quad (3)$$

where the quantity

$$\lambda := \frac{2}{3} \bar{k}_2 \bar{R}^5, \quad (4)$$

is another common way of expressing the tidal Love number for equal-mass binaries [13], while  $\Lambda := \lambda/\bar{M}^5$  is its dimensionless counterpart and was employed in [11].

A quasi-universal relation, which is also present at the level of equilibrium solutions of nonrotating models, is the one relating the tidal deformability and the stellar compactness shown in Fig. 3 for the five EOSs considered here. It is not difficult to express this rather tight correlation with a polynomial of the type

$$\log_{10}(\kappa_2^T) \simeq d_0 + d_1 C + d_2 C^2 + d_3 C^3, \quad (5)$$

where  $d_0 = 6.29$ ,  $d_1 = -37.41$ ,  $d_2 = 85.68$ ,  $d_3 = -101.07$  for stable models with  $C > 0.05$ . It is shown as a black solid line in Fig. 3. Note that this relation is valid over a range of compactness that is much larger than the one considered in the analysis here; more importantly, it effectively represents a way to map any measured quantity expressed in terms of  $\kappa_2^T$  to a quantity expressed in terms of  $C$ , and *vice versa*. Specifically, it introduces additional quasi-universal relations between frequencies [11, 15],

$$f_1 \approx c_0 + c_1 x + c_2 x^2 + c_3 x^3 \quad \text{kHz} \quad (6)$$

$$f_2 \approx 5.832 - 1.118 x \quad \text{kHz}, \quad (7)$$

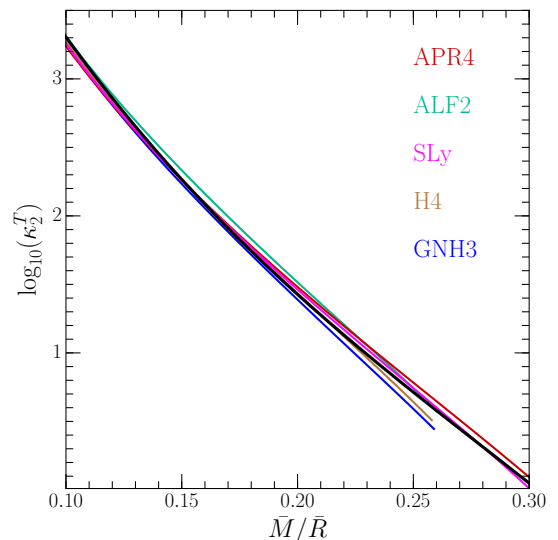


FIG. 3. Quasi-universal relation between the tidal deformability parameter and the stellar compactness for the four EOSs considered here and for APR4. Indicated with a black solid line is the fit given by Eq. (5).

where  $x := (\kappa_2^T)^{1/5}$ ,  $c_0 = 45.195$ ,  $c_1 = -43.484$ ,  $c_2 = 14.653$  and  $c_3 = -1.662$ .

Figure 4 shows instead the quasi-universal behavior found numerically. The left two panels refer to the  $f_1$ ,  $f_2$  frequencies when expressed as a function of the average compactness  $C = \bar{M}/\bar{R}$  of the neutron stars comprising the binary. Filled circles of different colors refer to equal-mass binaries with different EOSs. Black solid lines correspond to the analytic fits [11, 15]:

$$f_1 \approx a_0 + a_1 C + a_2 C^2 + a_3 C^3 \quad \text{kHz} \quad (8)$$

$$f_2 \approx b_0 + b_1 C + b_2 C^2 \quad \text{kHz}, \quad (9)$$

where  $a_0 = -35.17$ ,  $a_1 = 727.99$ ,  $a_2 = -4858.54$ ,  $a_3 = 10989.88$ ,  $b_0 = -3.12$ ,  $b_1 = 51.90$  and  $b_2 = -89.07$ . The two right panels show  $f_1$ ,  $f_2$  as a function of the tidal deformability parameter  $\kappa_2^T$ . As before, the black solid line shows the analytic fit. For a GW signal with a complete waveform SNR  $\simeq 14$ , the inspiral phase will determine  $\bar{M}$  with a  $1 - \sigma$  accuracy of about 11% [23], which is better than how accurately the same parameter can be measured from the postmerger phase alone. Therefore, the fitting functions for  $f_1$  and  $f_2$  show that the error in measuring  $f_1$  from observations of the postmerger phase can improve the accuracy with which the EOS parameter  $\lambda$  can be determined.

Figure 5, which is analogous to Fig. 1 in the main text, shows numerical waveforms and corresponding analytic fits for a series of low-mass binaries, i.e.,  $M = 2 \times 1.250 M_\odot$ . Note that in this case too, and apart from the short transient right after the merger (i.e., for  $0 \lesssim t \lesssim 3$  ms) the match between the numerical waveforms and the analytic ansatz is very good, both in the time and frequency domains. Obviously,

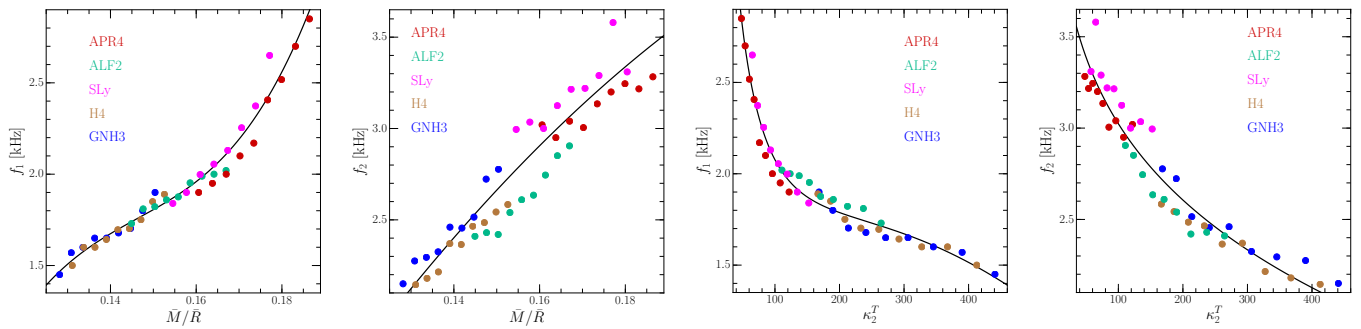


FIG. 4. *Left two panels:* Quasi-universal behavior of the  $f_1$ ,  $f_2$  frequencies when expressed as a function of the average compactness  $C = \bar{M}/R$  of the neutron stars comprising the binary. Filled circles of different colors refer to equal-mass binaries with different cold EOSs. The black solid line shows the analytic fit. *Right two panels:* The same as in the left two panels but when  $f_1$ ,  $f_2$  are expressed as a function of the tidal deformability parameter  $\kappa_2^T$ .

even better matches can be obtained if a better modelling is used for the transient phase (e.g., following the mechanical toy model discussed in Appendix A of [11]) or if the analytic ansatz is extended to include also very high-frequency components, namely, by including the modelling of the  $f_3$  frequency peak.

Finally, Fig. 6, complementary to Fig. 2 in the main text, shows errors in the reconstructed radii when the population of BNSs is characterised by a single value of the average mass, i.e., either  $\bar{M} = 1.250 M_\odot$  or  $\bar{M} = 1.325 M_\odot$ , for four different EOSs. Different values of shading refer to different number of binaries considered, i.e.,  $N = 20, 50, 100$ .

The errors clearly grow as a function of the tidal deformability. In view of the discussion relative to Fig. 3 and the quasi-universal relation (5), Fig. 6 essentially highlights a basic but important result: stellar radii measurements will be more accurate for stiff EOSs, while they will systematically suffer from larger uncertainties for soft EOSs.

We also performed a set of Monte-Carlo simulations where the masses were allowed to span a wider range, namely,  $[1.0, 2.0] M_\odot$ , for all four EOSs and the two mass distributions. Since we do not yet have numerical-relativity data on the  $f_2$  and compactness for masses beyond  $1.4 M_\odot$ , we extrapolated the quasi-universal relations to infer them. In these studies, there is no appreciable change in the radius errors for the GNH3 and H4 EOSs, but for ALF2 and SLy the radius errors rise to 7.4% (Gaussian) and 5.4% (uniform) and 12.0% (Gaussian) and 22.0% (uniform), respectively, at 90% confidence level. These large errors are not surprising since we expect waveforms from softer stars to damp faster and have the  $f_2$  peak at frequencies where the aLIGO sensitivity is worse. They warn us that our error estimates may change once numerical-relativity simulations for heavier stars become available.

Obviously, the Monte-Carlo results are more trustworthy than the Fisher results, but the latter are useful in providing a partial understanding of the former. It is also true that the size of the errors depends on the measurement method employed.

For instance, a coherent way of combining the EOS effects on full signal, from inspiral to postmerger, will influence those errors and impact EOS discernability.

A concluding remark will be dedicated to whether or not it is possible to find different and tighter correlations between the spectral properties of the postmerger signal and the radius at a given fixed mass. Results presented in Ref. [16], in fact, suggested that it is possible to find a quadratic quasi-universal relation between the  $f_2$  frequency and the radius of nonrotating neutron stars with a fixed mass of  $1.6 M_\odot$  [see Eq. (2) in Ref. [16], which the fit reported in the right panel of Fig. 4 in Ref. [16]].

When considering the results of our simulations, but also those of other groups, we are not able to confirm this behaviour; rather, we find that the scattering in the frequencies is quite large. This is shown in Fig. 7, which reports the values of the  $f_2$  frequencies for the various binaries considered in this work using the same colorcode adopted in all other figures, together with other data collected from the literature, with black crosses referring to the data reported in Refs. [16, 24] for equal-mass binaries with  $\bar{M} = 1.35 M_\odot$ , while filled squares refer to the data of Ref. [12] with  $\bar{M} = 1.35 M_\odot$  but not necessarily for equal-mass binaries (i.e.,  $\bar{M} = \frac{1}{2}(1.35 + 1.35)M_\odot$  and  $\bar{M} = \frac{1}{2}(1.25 + 1.45)M_\odot$ ). To help the comparison with Refs. [16, 24] we present the results for sequences with constant masses of  $\bar{M}/M_\odot = 1.200, 1.225, 1.250, 1.275, 1.300, 1.325, 1.350, 1.375,$  and  $1.400$ . The different sequences are connected with dotted lines, while the thick blue and red lines refer to our reference sequences having mass  $\bar{M}/M_\odot = 1.250$  and  $\bar{M}/M_\odot = 1.325$ , respectively.

As is apparent from Fig. 7, we cannot confirm that the quadratic fitting suggested by Eq. (2) of Ref. [16] is a good representation of the data, which instead show a rather large scatter. It is presently unclear what the origin of this discrepancy is, but our results, combined with those of other groups using fully general-relativistic numerical codes, warn against making use of quasi-universal relations for sequences of fixed

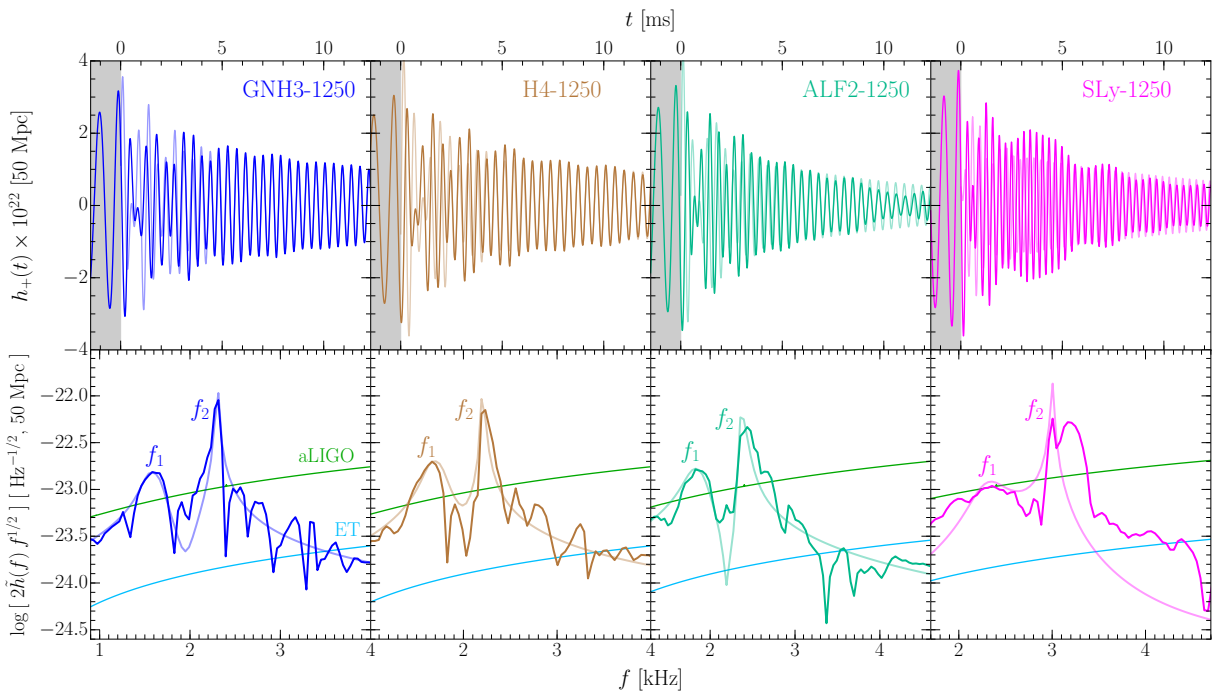


FIG. 5. The same as Fig. 1 in the main text, but for binaries with lower masses, i.e.,  $M = 2 \times 1.250 M_{\odot}$ . In this case too the match between the numerical waveforms and the analytic ansatz is very good; even better matches are expected if the analytic ansatz is extended to model also the  $f_3$  frequency peak.

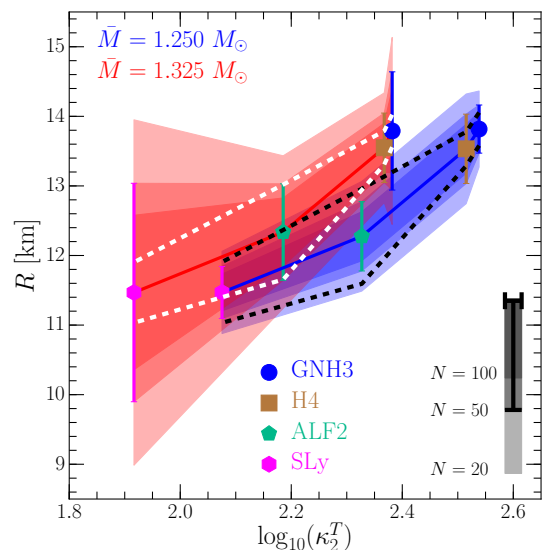


FIG. 6. Radius measurement error, at 90% confidence level, as a function of the tidal deformability when the population of BNSs, distributed uniformly in a comoving volume between 100 and 300 Mpc, is characterised by a single value of the average mass, i.e., either  $\bar{M} = 1.250 M_{\odot}$  or  $\bar{M} = 1.325 M_{\odot}$ , for the four EOSs studied here. Different values of shading refer to the different numbers of binaries considered, i.e.,  $N = 20, 50, 100$ . Note that soft EOSs have systematically larger uncertainties. Shown with dashed lines are the errors from the Fisher-matrix analysis for  $N = 50$ .

gravitational mass. Specifically, owing to the mass-related spread of the curves in Fig. 7 it is not obvious how for the population of 100 BNSs one might estimate  $R_{1.6}$  more accurately than the average radius of that population from the methods presented in this letter. However, for the nearby binary at 30 Mpc discussed above, since the BNS masses can be estimated to a high accuracy, it is possible to narrow that spread; this allows the determination of  $R_{1.6}$  for that case with an accuracy that rivals the estimation of the average radius deduced above.



binary	$f_1$	$\tau_1$	$f_2$	$\tau_2$	$\gamma_2$	$\xi_2$	$\alpha$	$\Delta f_1$	$\Delta f_2$	$\Delta C/C$	$\Delta f_2^{\text{MC}}$	$[\Delta R/R]^{\text{MC}}$
	[kHz]	[ms]	[kHz]	[ms]	[Hz <sup>2</sup> ]	[Hz <sup>3</sup> ]		[Hz]	[Hz]	[%]	[Hz]	[%]
GNH3-1250	1.60	2	2.30	23.45	38	-9.e2	0.46	371	29	1.0	14.3	1.8
H4-1250	1.65	5	2.22	20.45	-677	0.0	0.55	151	43	1.2	50	2.7
ALF2-1250	1.85	15	2.42	10.37	-3467	2.e4	0.55	66	133	3.4	62.5	3.0
SLy-1250	2.30	1	3.00	13.59	0	0.0	0.50	1683	82	2.2	52.0	2.4
GNH3-1325	1.70	2	2.45	23.45	342	5.e4	0.35	371	40	1.0	100	4.5
H4-1325	1.75	5	2.47	20.45	-1077	4.5e3	0.30	177	27	1.0	50	2.7
ALF2-1325	2.05	15	2.64	10.37	-863	2.5e4	0.50	79	60	1.6	97	4.0
SLy-1325	2.30	1	3.22	13.59	-617	5.5e4	0.50	1137	74	2.0	312	9.8

TABLE I. Parameter values for the analytic waveform models.  $\beta_2$  is adjusted to match numerical-relativity waveforms.  $\Delta f_{1,2}$  are Fisher-matrix  $1 - \sigma$  error estimates from postmerger signals in a single aLIGO detector for a reference population of 100 binaries with optimal orientation and sky position, a distance of 200 Mpc, and an integration time of 25 ms.  $\Delta C/C$  is deduced from  $\Delta f_2$  by error-propagation using quasi-universal relations. The errors in  $f_2$  and the average radius, at 90% confidence level, of a BNS population with identical component masses and EOS, distributed uniformly in volume between 100 Mpc and 300 Mpc, and averaged over orientation and sky position, obtained from Monte-Carlo simulations are listed in the last two columns, respectively.

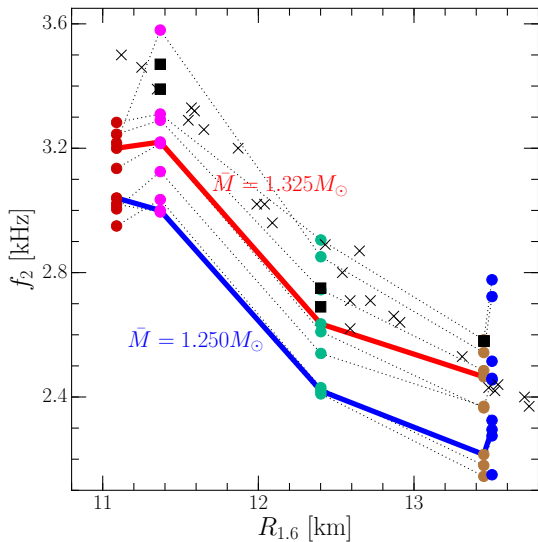


FIG. 7. Values of the  $f_2$  frequencies shown in terms of  $R_{1.6}$ , the radius of a nonrotating neutron star with  $\bar{M} = 1.6 M_\odot$ . The various filled circles refer to the  $f_2$  frequencies at masses  $\bar{M}/M_\odot = 1.200, 1.225, 1.250, 1.275, 1.300, 1.325, 1.350, 1.375,$  and  $1.400$ ; these sequences are connected with dotted lines, while the thick blue and red lines refer to our reference sequences having mass  $\bar{M}/M_\odot = 1.250$  and  $\bar{M}/M_\odot = 1.325$ , respectively. Indicated with black crosses is the data reported in Refs. [16, 24] for equal-mass binaries with  $\bar{M} = 1.35 M_\odot$ , while filled squares refer to the data of Ref. [12] with  $\bar{M} = \frac{1}{2}(1.35 + 1.35)M_\odot$  and  $\bar{M} = \frac{1}{2}(1.25 + 1.45)M_\odot$ . Note the large scatter across different masses.